Effect of Strength Mismatch on Fully Plastic Fields in Dissimilar Joints under Combined Loading

Hyungyil Lee* and Yun-Jae Kim**

(*Received July 26, 1997*)

Via detailed finite element limit analyses, plastic limit loads, rotation factors, and crack-tip stress field are investigated for a combined tension and bending of a plane strain single-edge -cracked bimaterial specimen. Limiting bimaterial specimens are considered, consisting of an elastic/perfectly plastic material bonded to an elastic material having the same elastic properties. The limit loads of bimaterial specimens are shown to be very close to those of homogeneous specimens, so that limit load information for homogeneous specimens can be used even for bimaterial specimens. A tractable, approximate elliptical yield locus is proposed, which fits the FE results within 1%, for all ranges of tension-to-bending ratios. The plastic rotation factor of bimaterial specimens can be higher than that of homogeneous specimens as much as 25%, when the specimen is subject to small tensile forces. Results from the present analysis is applied to the analysis of typical fracture testing specimens such as compact tension specimens. For both homogeneous and bimaterial specimens, larger tensile forces are associated with substantial loss of crack-tip constraint. Bimaterial specimens have as much as 2 times higher constraint than homogeneous specimens, due to plastic strength mismatch. Tractable closed form approximations for crack-tip stresses are proposed in terms of tension-to-bending ratio.

Key Words: Single-Edge-Cracked Specimen, Bimaterial, Combined Tension and Bending, Finite Element Analysis, Fully Plastic, Limit Load, Rotation Factor, Crack-Tip Constraint

1. Introduction

Defects in typical complex structures, if exist, are essentially subject to combined loadings (such as tension, bending and in-plane/out-of-plane shear loading). Therefore, assessment for structural integrity of such structures requires analyses of typical cracked-specimens under combined loadings. Among combinations of those loadings, the most interesting one would be combined tension and bending. One application would be fracture analyses of compact tension (CT) and pin-loaded single-edge-cracked (SEC) specimens. The cracks in such specimens are subject to combined tension and bending, and the tension-to-bending ratio depends on the relative crack depth to the specimen width. Another important structural application is the Line-Spring Model (LSM), proposed by Rice and Levy (1972) as a simplified but powerful tool for analyzing surface cracks in plates and shell-type geometries. The LSM requires analyses of SEC specimens under combined tension and bending in two limiting deformation conditions : analyses in the linear elastic regime and in the full yielding regime (White *et al.*, 1983). For homogeneous specimens, Lee and Parks (1993), and Kim (1993) provided a framework to determine fully plastic fields for such specimens with sufficiently deep cracks, based on perfect plasticity.

However, many structural components are produced by welding and/or bonding, and thus interface between two different materials is inherent for such components. Since the interface

* Department of Mechanical Engineering, Sogang University, Seoul, Korea.
** GKSS Research Center, Germany.

would be probably the most vulnerable spot for fracture in such components, mechanical performance would be limited due to interfacial fracture. To assess fracture of such components, knowledge of plastic limit loads and plastic rotation factors is essential, from which crack driving forces such as the J-integral and the crack-tip opening displacement can be estimated. For homogeneous specimens, these information can be easily obtained from handbooks. However, for bimaterial specimens, such information is not yet provided. More important information for assessing fracture is crack-tip stresses on which fracture strongly depends. Compared with the level of understanding of crack-tip stresses for homogeneous specimens, little is known for bimaterial specimens.

We, therefore, perform fully plastic analyses for combined tension and bending of the plane strain single-edge-cracked bimaterial specimen with sufficiently deep cracks, via detailed finite element (FE) limit analyses. We first estimate the variables related to fully plastic deformations, such as limit loads (yield locus) and plastic rotation factors. Such deformation-related variables can provide some useful information on crack driving forces such as evaluation of the J-integral and the crack-tip opening displacement.

On the other hand, it is well known that fracture process and thus fracture toughness depends on crack-tip strains and more importantly crack-tip stresses (McClintock, 1968 ; Rice and Tracy, 1969). In recent years, there appear more evidences that the crack-tip stress (constraint) significantly affects fracture toughness (Hancock, 1992 ; Du and Hancock, 1991 ; Parks, 1992 ; O' Dowd and Shih, 1991 ; 1992). Thus, to assess fracture, information on crack-tip stresses is essential. In the latter part of this paper, we investigate the crack-tip stress fields. Unlike deformation-related variables, crack-tip stresses strongly depends on the net-section tension-to-bending ratio, as will be shown in this paper. It will be shown that larger tensile force is associated with significant loss of crack-tip constraints. Moreover, being compared with homogeneous specimens, bimaterial specimens are associated with higher crack-tip constraints. The reason for higher crack-tip constraints in bimaterial specimens is fully discussed in this paper. Finally, a tractable closed-form approximation of crack-tip stresses is presented in terms of the net-section tension-to-bending ratio.

2. Finite Element Model for Limit Analyses

Consider combined tension and bending of a plane strain single-edge-cracked (SEC) bimaterial specimen with a sharp and deep interfacial crack lying between two different materials (Fig. 1(a)). For clarity, assume that two materials have the same elastic properties, but different plastic properties. Such case is typical for one class of important problems, namely, many welded ferritic or austenitic steels. For simplicity, consider a limiting case of the bimaterial specimen consisting of an elastic/perfectly plastic material bonded to an elastic material (Fig. 1(b)). Such case can be compared with another limiting case of homogeneous specimen consisting of an elastic/perfectly plastic material. The elastic/perfectly plastic material has a yield strength of σ_o which can be

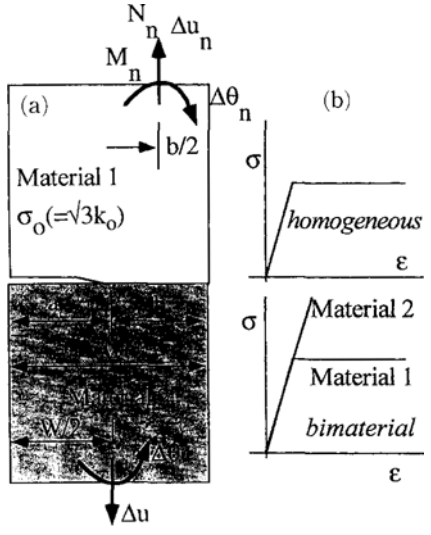

Fig. 1 (a) Plane strain single-edge-cracked (SEC) bimaterial specimen under combined tension and bending. (b) Material model considered in this paper.

related to the yield strength in shear by $k_o = \sigma_o/\sqrt{3}$. As shown in Fig. 1(a), the loads and deformations, N_n, M_n, u_n, and θ_n, are based on the net-section of the specimen. For compact notation throughout the text, the loading variables such as N_n and M_n, are normalized with respect to the limit loads for the uncracked specimen using k_o and the remaining ligament of the specimen, b :

$$\hat{N}_n = N_n/(2k_o b) \; ; \; \hat{M}_n = M_n/(0.5k_o b^2) \qquad (1)$$

Define a net-section loading ratio η_n as

$$\eta_n \equiv \frac{bN_n}{bN_n + M_n} = \frac{4\hat{N}_n}{4\hat{N}_n + \hat{M}_n} \qquad (2)$$

which measures the remotely applied tension-to-bending ratio. The value of η_n varies from 0 for pure bending ($\hat{N}_n = 0$), to 1 for pure tension ($\hat{M}_n = 0$). In the literature (Lee and Parks, 1993 ; Liu and Drugan, 1993), one can find another parameter for the bending-to-tension ratio, $\mu_n = M_n/(bN_n)$, which ranges from 0 for pure tension to ∞ for pure bending. The proposed η_n is related to μ_n as $\eta_n = 1/(1+\mu_n)$. The parameter η_n facilitates simple closed-form approximations for crack-tip parameters.

We performed limit analyses of the finite element (FE) model. A small strain continuum 2-dimensional FE model was employed. To avoid problems associated with incompressibility, reduced integration 8-node 2-D elements (element type CPE8R from the ABAQUS library, 1995) were used. The crack-tip is surrounded circumferentially by twelve fans of element in the first quadrant, and by six fans of elements in the second quadrant. There are 918 plane strain reduced integration 8-node elements, and 2899 nodes. The radial extent of the first crack-tip element is about 0.5×10^{-3} of the specimen-ligament b. A similar FE mesh can be found in the work of Lee and Parks (1993). *Combined displacement and rotation boundary conditions* were imposed on the top edge of this FE model, whereas fixed boundary conditions on the bottom edge. The magnitude of the applied deformation is made large enough to bring the specimen to its limiting load state, which can be determined from the reaction force and reaction moment corresponding to the combined displacement and rotation boundary conditions imposed on the top edge of SEC specimen FE model. Results are obtained for only one crack depth of $a/W = 0.5$. For all tension-to-bending ratios, FE results showed that this crack depth is sufficiently deep enough, so that deformations are confined only to the uncracked ligament.

3. Yield Locus

3.1 Homogeneous specimens

Limit loads from finite element (FE) limit analyses are shown in Fig. 2 with open circles. For the bending-dominant regime ($0 \le \hat{N}_n \le = 0.551$), the limit loads (yield locus) can be obtained from modified Green and Hundy slip line fields (Green and Hundy, 1956 ; Shiratori and Dodd, 1980 ; Shiratori and Miyoshi, 1980) :

$$\Phi = \hat{M}_n + 0.739\hat{N}_n^2 - 0.521\hat{N}_n - 1.261 = 0 \qquad (3)$$

For the tension-dominant regime ($0.551 \le \hat{N}_n \le 1$), Kim *et al.* (1996) proposed the elliptical

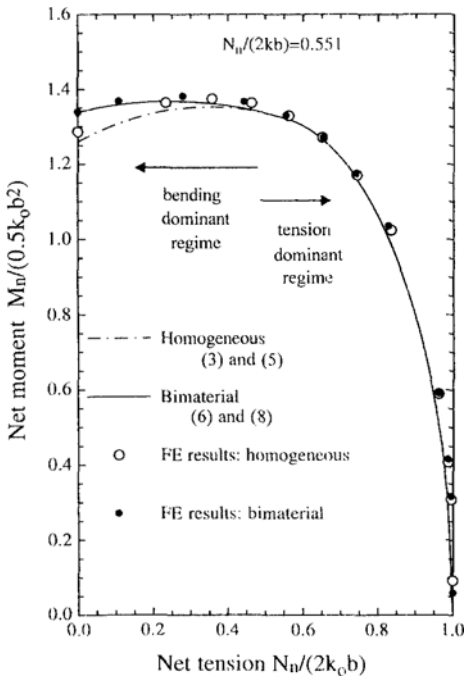

Fig. 2 Yield locus in the generalized net-section force space for deeply-cracked SEC specimens under combined tension and bending : homogeneous and bimaterial specimens.

yield locus in the form of

$$\Phi = A_1(\hat{M}_n - B_1)^2 + C_1(\hat{N}_n - D_1)^2 - 1 = 0 \quad (4)$$

Four unknown coefficients A_1, B_1, C_1 and D_1, are determined such that the ellipse smoothly matches the yield loci of the adjacent SLF solutions (from (3)) at the respective end points :

$$\left\{\begin{array}{lll} \hat{M}_n = 0 & \text{at} & \hat{N}_n = 1 \\ \partial\hat{N}_n/\partial\hat{M}_n = 0 & \text{at} & \hat{N}_n = 1 \\ \hat{M}_n = 1.323 & \text{at} & \hat{N}_n = 0.551 \\ \partial\hat{N}_n/\partial\hat{M}_n = -1/0.294 & \text{at} & \hat{N}_n = 0.551 \end{array}\right\}$$

The resulting ellipse is

$$\Phi = 0.564\hat{M}_n^2 + 3.926(\hat{N}_n - 0.495)^2 - 1 = 0 \quad (5)$$

Approximate ellipses (3) and (5) are compared with the FE results in Fig. 2. It shows that they agree remarkably well with the FE results, within 1%.

3.2 Bimaterial specimens

Limit loads from finite element (FE) limit analyses for bimaterial specimens consisting of an elastic/perfectly plastic material bonded to an elastic material are shown in Fig. 2 with closed circles. At the first glance, it can be seen that the limit loads of bimaterial specimens are almost same as those of homogeneous specimens, in the tension-dominant regime ($0.551 \le \hat{N}_n \le 1$). Thus, in the tension-dominant regime ($0.551 \le \hat{N}_n \le 1$), the same approximate elliptical yield locus can be used for both homogeneous and bimaterial specimens :

$$\Phi = 0.564\hat{M}_n^2 + 3.926(\hat{N}_n - 0.495)^2 - 1 = 0 \quad (6)$$

However, for the bending-dominant regime ($0 \le \hat{N}_n \le 0.551$), the limit loads of bimaterial specimens are *slightly* higher than those of homogeneous specimens. For that regime, we propose an elliptical yield locus in the following form :

$$\Phi = A_2\hat{M}_n^2 + B_2(\hat{N}_n - C_2)^2 - 1 = 0 \quad (7)$$

Three unknown coefficients, A_2, B_2 and C_2, are determined such that the ellipse smoothly matches the yield locus of the tension-dominant regime (6) at the one end point ($\hat{N}_n = 0.551$), and matches the FE result at the other end point ($\hat{N}_n = 0$) :

$$\left\{\begin{array}{lll} \hat{M}_n = 1.370 & \text{at} & \hat{N}_n = 0 \\ \hat{M}_n = 1.323 & \text{at} & \hat{N}_n = 0.551 \\ \partial\hat{N}_n/\partial\hat{M}_n = -1/0.294 & \text{at} & \hat{N}_n = 0.551 \end{array}\right\}$$

The resulting ellipse is

$$\Phi = 0.526\hat{M}_n^2 + 0.524(\hat{N}_n - 0.161)^2 - 1 \quad (8)$$

Note that the proposed elliptical yield loci, (6) and (8), automatically satisfy the convexity condition for the yield surface. Approximate ellipses (6) and (8) agree remarkably well with the FE results, within 1%, as shown in Fig. 2.

One interesting point is that the limit loads of bimaterial specimens are very close to those of homogeneous specimens. The difference is only in bending-dominant regime, but it is still within 5%. In most of bending-dominant regime, the difference is negligible. Since we considered an extreme bimaterial combination (elastic-plastic/elastic), one can conclude that the limit loads of general bimaterial specimens (consisting of two elastic-plastic materials) would be even closer to those of homogeneous specimens. Therefore, using limit loads for homogeneous specimens for bimaterial specimens would not give serious errors.

4. Plastic Crack-Tip Opening Displacement

It is a common practice that the crack-tip opening displacement (CTOD or δ_t) is decomposed operationally into its linear-elastic and plastic parts : $\delta_t = \delta_t^{(e)} + \delta_t^{(p)}$. The magnitude of $\delta_t^{(e)}$ for both homogeneous and bimaterial specimens can be obtained easily from handbooks. However, in most of practical cases where gross plasticity prevails, the magnitude of $\delta_t^{(p)}$ will dominate that of $\delta_t^{(e)}$, which is focused in this paper.

4.1 Plastic CTOD

To fix the idea, we have to introduce the reference point for measuring displacement and rotation. For convenience, define the plastic displacement and rotation at the mid-specimen, $u^{(p)}$ and $\theta^{(p)}$ (Fig. 1(a)), as the reference load-point displacement and rotation. The displacement and

rotation at the other point in the specimen can be obtained from kinematics of rigid body rotations. For instance, the displacement and rotation at the mid-net-section, $u_n^{(p)}$ and $\theta_n^{(p)}$(Fig. 1(a)), are related to $u^{(p)}$ and $\theta^{(p)}$ as

$$u_n^{(p)} = u^{(p)} - \frac{a}{2}\theta^{(p)} \; ; \; \theta_n^{(p)} = \theta^{(p)} \tag{9}$$

For SEN specimens with a sufficiently deep crack (for both homogeneous and bimaterial specimens), there exists a simple relationship between the plastic component of the *CTOD* increment, $\Delta\delta_t^{(p)}$, and the plastic load-point displacement and rotation increments, $\Delta u^{(p)}$ and $\Delta\theta^{(p)}$:

$$\Delta\delta_t^{(p)} = \Delta u^{(p)} + \left(\frac{W}{2} - a\right)\Delta\theta^{(p)} \tag{10}$$

However, note that, for shallow cracks, the relation (10) does not hold due to shoulder deformation, as investigated by Lee and Parks (1993) for homogeneous specimens. Since the FE model in the present investigation assumed $a/W=0.5$, (10) gives $\Delta\delta_t^{(p)} = \Delta u^{(p)}$. Figure 3 confirms the above relationship, showing comparisons of $\Delta\delta_t^{(p)}$ from the FE limit analyses with the prediction (10). From the FE model, $\delta_t^{(p)}$ was measured as follows. For instance, for $a/W=0.5$, the crack-tip of the continuum FE models comprises 37 independent but initially coincident nodes, giving a $1/r$-strain singularity. The first node belonged to the interface. The incremental distance under full plasticity in the y-direction from the last (37th) node from the first node was regarded as $\Delta\delta_t^{(p)}$. Figure 3 shows that, for all ranges of tension-to-bending ratios, the prediction (10) differ from the FE results by less than 1%

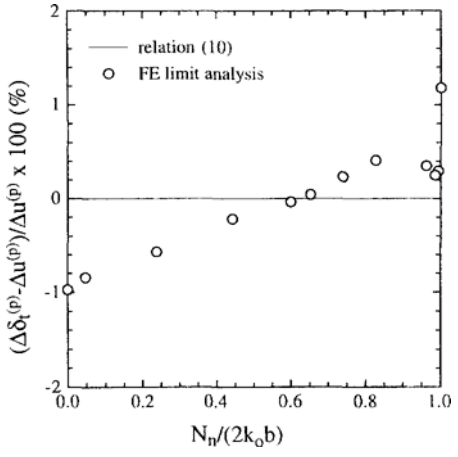

Fig. 3 Plastic crack-tip opening displacement increment, $\Delta\delta_t^{(p)}$, as a function of load-point displacement and rotation, for SEC specimens under combined tension and bending.

Equation (10) can be useful when one knows or measures the displacement and rotation. However, in general, it is easier to measure the force and moment. When the force and moment are known, the corresponding ratio of displacement to rotation can be determined from the yield locus proposed in the previous section, via the normality rule.

4.2 Plastic rotation factor r_p

The plastic crack mouth opening displacement (CMOD) increment, $\Delta\delta_m^{(p)}$, is related to $\Delta\delta_t^{(p)}$ by the following equation

$$\Delta\delta_t^{(p)} = \frac{r_p b \Delta\delta_m^{(p)}}{r_p b + a} \tag{11}$$

where r_p is the plastic rotation factor. Thus, if r_p is known, $\delta_t^{(p)}$ can be determined by measuring $\delta_m^{(p)}$. Recasting (11) gives

$$r_p = \frac{a\Delta\delta_t^{(p)}}{b(\Delta\delta_m^{(p)} - \Delta\delta_t^{(p)})} \tag{12}$$

The values of $\Delta\delta_m^{(p)}$ were measured in a similar manner to those of $\Delta\delta_t^{(p)}$.

For homogeneous specimens, Lee and Parks (1993) provided r_p for a wide range of the crack depth a/W. Among their results, the results for deep cracks ($a/W=0.5$) are shown in Fig. 4, in terms of the net-section loading ratio η_n defined in (2). In the limiting case of pure tension ($\eta_n=1$), $\Delta\delta_t^{(p)} = \Delta\delta_m^{(p)}$ and thus $r_p \to \infty$. Thus, for clear presentation, Fig. 4 presents the values of $1/r_p$ instead of the values of r_p. Figure 4 also includes the FE results of bimaterial specimens. For the tension-dominant regime ($0.63 < \eta_n < 1$), the values of r_p of bimaterial specimens are similar to those of homogeneous specimens. For the bending-dominant regime, the values of r_p of bimaterial specimens are higher than those of homogeneous specimens. The difference is as much as 25% at pure bending ($\eta_n=0$), where the values for homogeneous and bimaterial specimens

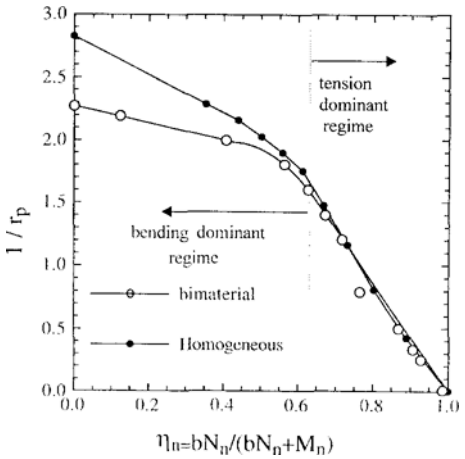

Fig. 4 Plastic rotation factor r_p for SEC specimens, as a function of net-section tension-to bending ratios η_n : homogeneous and bimaterial specimens.

are r_p=0.370 and r_p=0.439, respectively. Therefore, if one estimates the CTOD from the measured CMOD together with r_p from homogeneous specimens, (s)he will obtain either similar or lower CTOD values for bimaterial specimens, depending on the loading ratio.

Up to now, results are obtained for the SEC specimens under combined tension and bending. Such results can be immediately applied to one of popular fracture testing specimens, a compact tension (CT) specimen.

5. Compact Tension Bi-Material Specimens

Consider a compact tension (CT) homogeneous (bimaterial) specimen consisting of an elastic/perfectly plastic material bonded to an elastic material as shown in Fig. 5. The crack-tip in such specimen is subject to combined tension and bending, depending on the crack depth. From Fig. 5, static equilibrium gives the net-section force and moment in terms of the load line force P as

$$N_n = P \ ; \ M_n = P \cdot \left(a + \frac{b}{2}\right) \tag{13}$$

Thus, the net-section loading ratio η_n defined in (2) has the form of

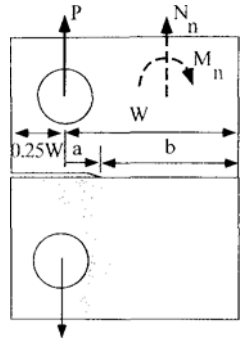

Fig. 5 Plane strain compact tension (CT) bimaterial specimen.

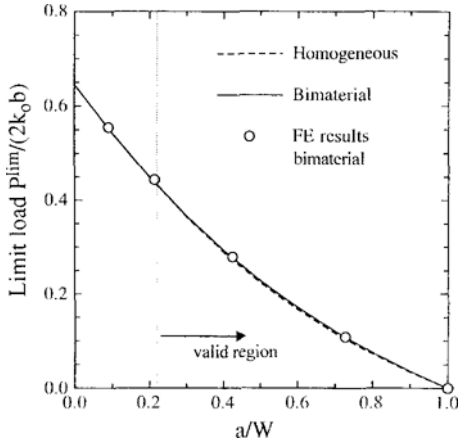

Fig. 6 Variations of plastic limit load P^{lim} with the crack depth a/W, for CT specimens : homogeneous and bimaterial specimens.

$$\eta_n = \frac{2(1-a/W)}{(3-a/W)} \tag{14}$$

When $a/W \to 0$ and 1, $\eta_n \to 0.67$ and 0, respectively. Since the bending-dominant regime covers $0 \le \eta_n \le 0.63$ as noted in the previous section, the whole range of a/W corresponds to the bending-dominant regime.

Figure 6 shows variations of the limit loads P^{lim} with a/W, for both homogeneous and bimaterial CT specimens. For homogeneous CT specimens, the results are obtained from the modified Green and Hundy solutions (Green and Hundy, 1956 ; Shiratori and Dodd, 1980 ; Shiratori and Miyoshi, 1980). On the other hand, for bimaterial CT specimens, the yield locus (8) together with static constraint (13) are used to evaluate P^{lim}. It is shown in Fig. 6 that both

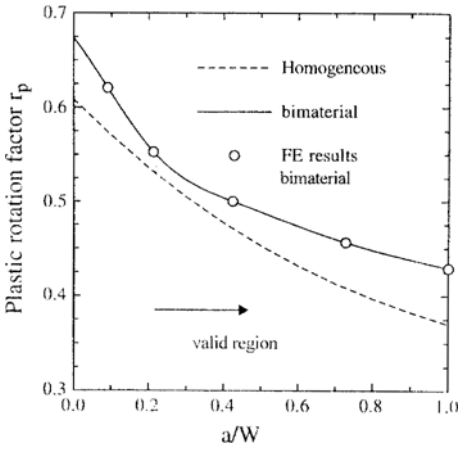

Fig. 7 Variations of plastic rotation factor r_p with the crack depth a/W, for CT specimens : homogeneous and bimaterial specimens.

curves almost coincide. *Therefore, the equation of limit loads for homogeneous CT specimens*, (13), *can be also used for bimaterial specimens*. Note that Wu *et al.* (1990) argued that, when the crack length a/W decreases to $a/W<0.22$ for homogeneous specimens, the front surface will affect deformation fields, in a similar fashion to the deformation in shallow-cracked bending specimens. It is likely that the same restriction is applied to CT bimaterial specimens, and that the present analysis can be applied only when $a/W>0.22$. Such limiting value of a/W is shown in Fig. 6.

Figure 7 shows the variation of the plastic rotation factor r_p on a/W, for homogeneous and bimaterial specimens. The values of bimaterial specimens are higher than those of homogeneous specimen for all ranges of a/W. The difference increases with a/W, and can be as much as 25% at $a/W=1$. Therefore, if one estimates the CTOD from the measured CMOD together with r_p from homogeneous CT specimens, (s)he will obtain lower CTOD values for bimaterial CT specimens.

6. Crack-Tip Stress Fields

Before we proceed, two points are worth noting. The first one is that, in the context of perfect plasticity, the crack-tip stresses taken from the FE results are not so sensitive to the location r, as long as r is sufficiently smaller than the ligament b. In this paper, the crack-tip stresses presented in the subsequent sections are measured at $r=0.1\times10^{-2}b$. The second point is that, for perfectly plastic materials, crack tip stress fields can be most vividly visualized by slip line fields composed by three basic fields : a centered fan, constant stress sector and elastic sector. The stresses in each sector can be obtained from slip line field theory.

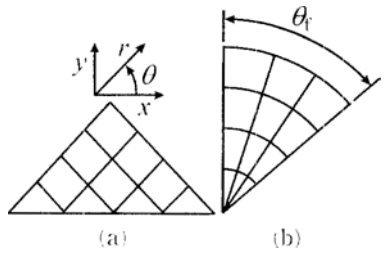

Fig. 8 Basic elements for asymptotic crack-tip slip line fields : (a) constant stress (C. S.) sector, and (b) deforming centered fan sector.

For instance, in the *centered fan* (Fig. 8(a)), yielding occurs due to the shear stress of $|\sigma_{r\theta}|=k$ where k denotes the yield shear strength of the plastic material, and the hydrostatic stress σ_m varies linearly with the angular orientation, according to the Hencky equation, $d\sigma_m=-2kd\theta$. Moreover, the values of the hoop stress $\sigma_{\theta\theta}$ and the radial stress σ_{rr} are the same as that of σ_m :

$$|\sigma_{r\theta}|=k\ ;\ \sigma_{\theta\theta}(\theta)=\sigma_{rr}(\theta)=\sigma_m(\theta)$$
$$d\sigma_m(\theta)=-2kd\theta \tag{15}$$

In the *constant stress* (C. S.) sector (Fig. 8(b)), the stresses in the cartesian coordinates are constant :

$$\sigma_{yy}=\sigma_{xx}+2k=\sigma_m+k=\text{constant}$$
$$|\sigma_{xy}|=0 \tag{16}$$

Or, in the polar coordinates,

$$\sigma_{\theta\theta}=k\cos2(\theta+\theta_o)+C\ ;$$
$$\sigma_{rr}=-k\cos2(\theta+\theta_o)+C\ ;$$
$$\sigma_{r\theta}=k\sin2(\theta+\theta_o)\ ;\ \sigma_m=C \tag{17}$$

where the constants, θ_o and C, should be determined from the boundary conditions. Note that the hydrostatic stress σ_m can increase only in the fan sector, according to the Hencky equation.

Therefore, the magnitude of σ_m (thus crack-tip constraint) depends on the angular size of the fan (θ_f in Fig. 8(b)). Larger θ_f is associated with higher σ_m at the crack-tip and thus higher constraint.

In the following section, the crack-tip fields obtained from the FE limit analyses will be schematically presented in terms of slip line fields.

6.1 Homogeneous specimens

Angular variations for crack-tip stresses

Figure 9(a) and (b) show angular variations of (a) the hydrostatic stress σ_m and (b) the hoop stress $\sigma_{\theta\theta}$ for homogeneous specimens, for various tension-to-bending ratios. Note that $\eta_n=0$ and 1 corresponds to "pure bending" and "pure tension", respectively. Results in Fig. 9 shows that, for all ranges of the net-section tension-to-bending ratios, the value of σ_m is constant from $\theta=0$ to $\theta=45°$, but decreases linearly with θ at $\theta\geq 45°$. In terms of slip line fields, it can be described that the constant stress sector resides from $\theta=45°$ to $\theta=0$ (where σ_m remains constant) and the centered fan field (where σ_m varies according to the Hencky equation) extends angularly from $\theta=45°$ to the angular position where yield conditions are violated. The elastic sector then connects the crack flank to the fan. Such asymptotic near-tip slip line field is depicted in Fig. 9(b), and will be termed here as a "partial Prandtl field".

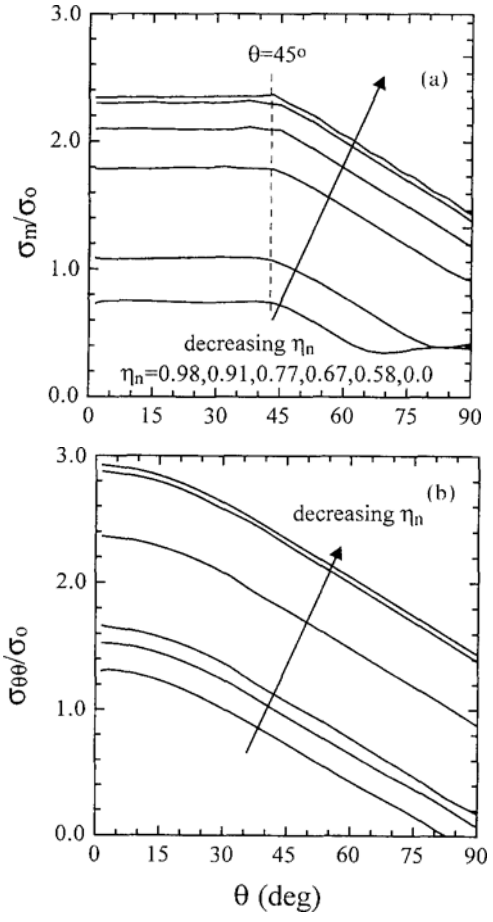

Fig. 9 Angular variations of (a) the hydrostatic stress σ_m and (b) the hoop stress $\sigma_{\theta\theta}$ for homogeneous SEN specimens under combined tension and bending. See Eq (2) for the definition of η_n.

Note that, about three decades ago, Green and Hundy (1956), and Ewing (1968) have already imposed such hypothesis, and recently Lee and Parks (1993) also observed such field in their FE analyses. Results in Fig. 9 also shows that, up to the certain tension-to-bending, angular variations of σ_m are negligible. Interpreting in terms of slip line fields, the angular size of the elastic sector in Fig. 10, and thus the size of the fan (θ_f), remains constant. However, larger tensile forces moves the curve downward quickly, indicating appreciable loss of crack-tip constraints. It means that the size of the elastic sector increases quickly, and thus the fan size decreases. Such tendency will be quantitatively characterized in the next section.

One more notable point is that stress distribution in the constant stress sector gives zero shear stress along the cracked line, $\sigma_{r\theta}=0$ at $\theta=0$, corresponding to the Mode I loading condition.

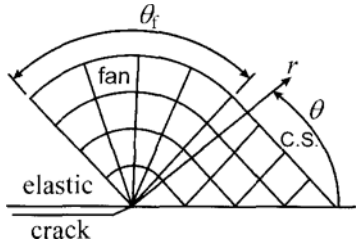

Fig. 10 Asymptotic crack-tip slip line field for homogeneous specimens (partial Prandtl field).

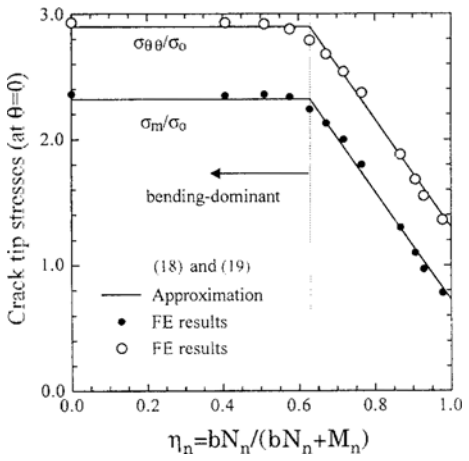

Fig. 11 Variation of the hydrostatic stress and the tensile stress directly ahead of the crack-tip, $(\sigma_m)_{\theta=0}$ and $(\sigma_{\theta\theta})_{\theta=0}$, in terms of the net-section loading ratio η_n.

However, for bimaterial specimens, $\sigma_{r\theta}$ at $\theta=0$ (interface) is no longer zero, which will be explained later. It will provide the key to explain the difference of crack-tip stresses between homogeneous and bimaterial specimens.

Stresses directly ahead of the crack-tip

Figure 11 shows the variation of the hydrostatic stress and the tensile stress directly ahead of the crack-tip, $(\sigma_m)_{\theta=0}$ and $(\sigma_{\theta\theta})_{\theta=0}$, in terms of the net-section loading ratio η_n (defined in (2)). Results in Fig. 11 suggest the simple closed form approximations of $(\sigma_m)_{\theta=0}$ and $(\sigma_{\theta\theta})_{\theta=0}$ as follows :

For the bending-dominant regime $(0\leq\eta_n\leq0.63)$,

$$(\sigma_m(\eta_n)/\sigma_o)_{\theta=0}=2.32,$$
$$(\sigma_{\theta\theta}(\eta_n)/\sigma_o)_{\theta=0}=(\sigma_m(\eta_n)/\sigma_o)_{\theta=0}+1/\sqrt{3}=2.90 \quad (18)$$

Note that the values of $(\sigma_m)_{\theta=0}$ and $(\sigma_{\theta\theta})_{\theta=0}$ remain constant in this regime. On the other hand, for the tension-dominant regime $(0.63\leq\eta_n\leq1)$,

$$(\sigma_m(\eta_n)/\sigma_o)_{\theta=0}=-4.32\eta_n+5.04$$
$$(\sigma_{\theta\theta}(\eta_n)/\sigma_o)_{\theta=0}=(\sigma_m(\eta_n)/\sigma_o)_{\theta=0}+1/\sqrt{3}$$
$$=-4.32\eta_n+5.62 \quad (19)$$

The values of $(\sigma_m)_{\theta=0}$ and $(\sigma_{\theta\theta})_{\theta=0}$ decreases linearly with η_n, and converges to the values for pure tension, $(\sigma_m)_{\theta=0}\doteq0.73$ and $(\sigma_{\theta\theta})_{\theta=0}\doteq1.30$. Therefore, a variety of crack-tip constraints can be obtained by changing the net-section tension-to-bending ratio of the SEN specimen.

A crack in the compact tension (CT) specimen is subject to combined bending and tension, depending on the crack depth a/W. However, as shown in Sec. 5, all range of the crack depth a/W corresponds to the bending-dominant regime. The present study verifies the common knowledge that, for the CT specimen, the crack-tip constraint is almost constant, regardless of a/W.

6.2 Bimaterial specimens

Angular variations for crack-tip stresses

Figures 12(a) and (b) shows the FE results of angular variations of (a) the hydrostatic stress σ_m and (b) the hoop stress $\sigma_{\theta\theta}$ for bimaterial specimens, for selected tension-to-bending ratios. One notable point is that the value of σ_m varies linearly with θ, even at $0\leq\theta\leq45°$. Note that, for homogeneous specimens, it was constant, as shown in Fig. 9(a). Interpreting in terms of the slip line field, the deforming fan field extends up to the interface, as schematically depicted in Fig. 13. Thus, at the interface $(\theta=0)$, the magnitude of the shear stress is its maximum possible value of k_o, $(\sigma_{r\theta})_{\theta=0}=k_o$. Compared with those of homogeneous specimens, bimaterial specimens have larger fan size. As noted, larger angular size of the fan is associated with higher stress triaxiality (crack-tip constraint). Thus, for all rang of the net-section tension-to-bending ratios, bimaterials specimens are subject to higher crack-tip constraints than homogeneous specimens. Such higher constraint for bimaterial specimens has been studied by Kim and Lee (1996), in the context of small scale yielding. They found that the plastic strength mismatch (defined as the ratio of the yield strengths of two materials) strongly affects the crack-tip constraint. Starting from homogeneous material (no strength mismatch), the crack-tip constraints first increases, as strength mismatch increases, and then remains constant. The present bimaterial combination corresponds to the extreme strength mismatching (since one material is elastic).

Another notable point is that the dependence of

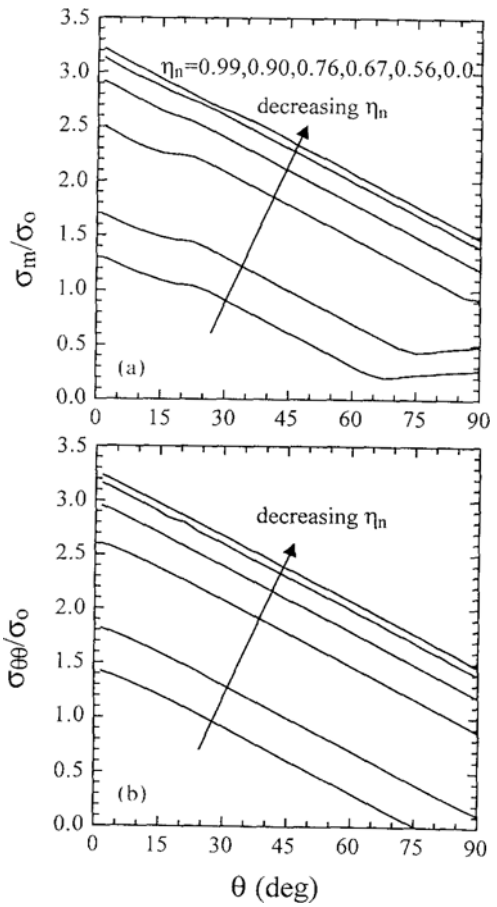

Fig. 12 Angular variations of (a) the hydrostatic stress σ_m and (b) the hoop stress $\sigma_{\theta\theta}$ for bimaterial SEN specimens under combined tension and bending.

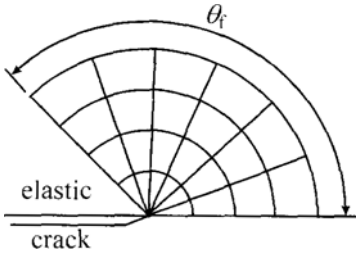

Fig. 13 Asymptotic crack-tip slip line field for bimaterial specimens (deforming fan field).

$(\sigma_m)_{\theta=0}$ and $(\sigma_{\theta\theta})_{\theta=0}$ on η_n for bimaterial specimens is very similar to that for homogeneous specimens.

Crack-tip stresses at the interface

Figures 14(a) and (b) show the FE results of

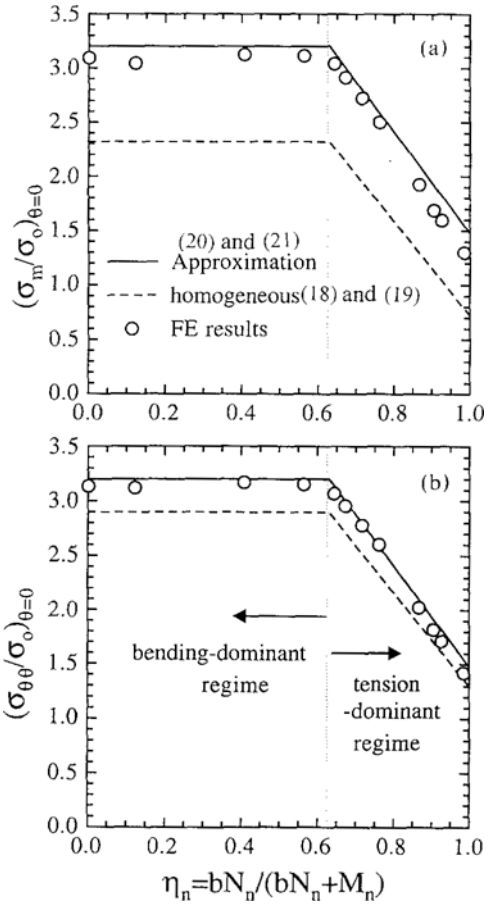

Fig. 14 Variation of the hydrostatic stress and the tensile stress directly ahead of the crack-tip. (a) $(\sigma_m)_{\theta=0}$ and (b) $(\sigma_{\theta\theta})_{\theta=0}$, in terms of the net-section loading ratio η_n.

the hydrostatic stress and the tensile stress at the interface, $(\sigma_m)_{\theta=0}$ and $(\sigma_{\theta\theta})_{\theta=0}$, in terms of η_n. For comparisons, Figs. 14(a) and (b) also include the approximations for homogeneous specimens, defined in (18) and (19). As explained qualitatively in the previous section, bimaterials specimens are subject to higher crack-tip constraints than homogeneous specimens, for all range of the net-section tension-to-bending ratios. In the bending-dominant regime, the hydrostatic stress is about 40% higher.

Since the dependence of $(\sigma_m)_{\theta=0}$ and $(\sigma_{\theta\theta})_{\theta=0}$ on η_n for bimaterial specimens is very similar to that for homogeneous specimen, we propose the following closed form approximations for

bimaterial specimens.

For the bending-dominant regime ($0 \leq \eta_n \leq 0.63$),

$$(\sigma_m(\eta_n)/\sigma_o)_{\theta=0} = (\sigma_{\theta\theta}(\eta_n)/\sigma_o)_{\theta=0} = 3.20 \quad (20)$$

For the tension-dominant regime ($0.63 \leq \eta_n \leq 1$),

$$(\sigma_m(\eta_n)/\sigma_o)_{\theta=0} = (\sigma_{\theta\theta}(\eta_n)/\sigma_o)_{\theta=0} = -4.60\eta_n + 6.10 \quad (21)$$

7. Concluding Remarks

Via detailed finite element (FE) limit analyses, plastic limit loads, plastic rotation factors and crack-tip stresses are investigated for combined tension and bending of plane strain single-edge-cracked bimaterial specimens. A limiting case bimaterial specimens is considered, consisting of an elastic/perfectly plastic material bonded to an elastic material having the same elastic properties. Results are compared with those for homogeneous specimens consisting of an elastic/perfectly plastic material.

The limit loads of bimaterial specimens are very close to those of homogeneous specimens, so that limit load information for homogeneous specimens can be used even for bimaterial specimens. A tractable, approximate elliptical yield locus is proposed, which fits the FE results within 1%, for all ranges of tension-to-bending ratios. The plastic rotation factor r_p for bimaterial specimens can be higher than that for homogeneous specimens as much as 25%, when the specimen is subject to small tensile forces. Results from the present analysis is applied to analysis of typical fracture testing specimens, compact tension (CT) specimens.

For both homogeneous and bimaterial specimens, larger tensile forces are associated with substantial loss of crack-tip constraint. However, for smaller tensile forces, the crack-tip constraint remains almost constant. Bimaterial specimens have as much as 2 times higher constraint than homogeneous specimens, due to plastic strength mismatch. Tractable closed form approximations for crack-tip stresses are proposed in terms of bending-to-tension ratio, for both homogeneous and bimaterial specimens.

Up to now, enormous results are published and much understandings have been achieved for homogeneous materials. Such results and understandings provide better assessment procedures for structural components. However, many structural components are produced by welding or bonding of similar or dissimilar materials, and since fracture of such components is likely to occur in welded areas, existing results for homogeneous materials cannot be applied to such welded components. Therefore, results in the present study are very useful to assess fracture toughness of such components. In general, however, structural components have flaws in the form of surface cracks. For homogeneous materials, the Line-Spring Model (LSM) has been proven to be an efficient and powerful tool to analyze surface cracks in plate/shell-like structural components (Hauf *et al.*, 1995; Kim, 1993; Lee and Parks, 1995). Following the idea explored for homogeneous materials, the present results need to be extended to apply the LSM to welded (bonded) components.

Acknowledgments

The authors are grateful for the support provided by a grant from the Korea Science & Engineering Foundation, and Safety and Structural Integrity Research Center.

References

ABAQUS *User's Manual*, 1995, Version 5.5, Hibbitt, Karlsson and Sorensen, Inc., Pawtucket, RI.

Du, Z. Z. and Hancock, J. W., 1991, "The Effect of Non-Singular Stresses on Crack Tip Constraints," *Journal of the Mechanics and Physics of Solids*, Vol. 39, 555~567.

Ewing, D. J. F, 1968, "Calculations on the Bending of Rigid/Plastic Notched Bars," *Journal of the Mechanics and Physics of Solids*, Vol. 16, pp. 205~213.

Green, A. P. and Hundy, B. B., 1956, "Initial Plastic Yielding in Notch Bend Tests," *Journal of the Mechanics and Physics of Solids*, Vol. 4, pp. 128~144.

Hancock, J. W., 1992, "Constraint and Stress State Effects in Elastic-Plastic Crack-Tip Fields," in *Topics in Fracture and Fatigue*, A. S. Argon (ed.), Springer-Verlag, 99~144.

Hauf, D. E., Parks, D. M. and Lee, H., 1995, "A Modified Effective Crack-Length Formulation in Elastic-Plastic Fracture Mechanics," *Mechanics of Materials*, Vol. 20, pp. 273~289.

Kim, Y.-J., 1993, *Modelling Fully Plastic, Plane Strain Crack Growth*, Ph . D. Dissertation, Department of Mechanical Engineering, Massachusetts Institute of Technology.

Kim, Y.-J., McClintock, F. A. and Parks, D. M., 1996, Yield Locus in Deep, "Single-Face-Cracked Specimens Under Combined Bending and Tension," Brief Note, *Journal of Applied Mechanics*, Vol. 63, pp. 1045~1047.

Kim, Y. J. and Lee, H., 1996, "On the Constraint of Elastic-Plastic Interfacial Cracks in Bimaterials," *in Proceedings of the KSME Materials and Fracture Division*, 41~46.

Lee, H. and Parks, D. M., 1993, "Fully Plastic Analyses of Plane Strain Single-Edge-Cracked Specimens Subject to Combined Tension and Bending," *International Journal of Fracture*, Vol. 63, pp. 329~349.

Lee, H. and Parks, D. M., 1995, "Enhanced Elastic-Plastic Line-Spring Finite Element," *International Journal of Solids and Structures*, Vol. 32, pp. 2393~2418.

Liu, N. and Drugan, W. J., 1993, "Finite Element Solutions of Crack Growth in Incompressible elastic-Plastic Solids with Various Yielding Extents and Loadings : Detailed Comparisons with Analytical Solutions," *International Journal of Fracture*, Vol. 59, pp. 265~289.

McClintock, F. A., 1968, "A Criterion for Ductile Fracture by Growth of Holes," *Journal of Applied Mechanics*, Vol. 35, pp. 363~371.

O'Dowd, N. P. and Shih, C. F., 1991, "Family of Crack-Tip Fields Characterized by a Triaxiality Parameter : Part Ⅰ — Structure of Fields," *Journal of the Mechanics and Physics of Solids*, Vol. 39, pp. 989~1015.

O'Dowd, N. P. and Shih, C. F., 1992, "Family of Crack-Tip Fields Characterized by a Triaxiality Parameter : Part Ⅱ — Fracture Applications," *Journal of the Mechanics and Physics of Solids*, Vol. 40, pp. 939~963.

Parks, D. M., 1992, "Advances in characterization of elastic-plastic crack-tip fields," in *Topics in Fracture and Fatigue*, Argon, A. S., (ed)., Springer-Verlag, 59~98.

Rice, J. R. and Tracey, D. M., 1969, "On the Ductile Enlargement of Voids in Triaxial Stress Fields," *Journal of the Mechanics and Physics of Solids*, Vol. 17, pp. 201~217.

Rice, J. R., 1972, "The Line Spring Model for Surface Flaws," *The Surface Crack : Physical Problems and Computational Solutions*, Swedlow, J. L., (ed)., American Society of Mechanical Engineers, New York, 171~185.

Rice, J. R. and Levy, N., 1972, "The Part-Through Surface Cracks in an Elastic Plates," *Journal of Applied Mechanics*, Vol. 39, pp. 185~194.

Shiratori, M. and Dodd, B., 1980, "Effect of Deep Wedge-Shaped Notches of Small Flank Angle on Plastic Failure," *International Journal of Mechanical Sciences*, Vol. 22, pp. 127~131.

Shiratori, M. and Miyoshi, T., 1980, "Evaluation of Constraint Factor and J-integral for Single-Edge Notched Specimen," in *Proceedings of the Third International Conference on the Mechanical Behavior of Materials*, Vol. 3, Pergamon Press, New York, pp. 425~434.

White, C. S., Ritchie R. O. and Parks, D. M., 1983, "Ductile Growth of Part-Through Surface Cracks : Experiment and Analysis," in *Elastic-Plastic Fracture*, ASTM STP 803, American Society for Testing and Materials, Ⅰ-384—Ⅰ-409.

Wu, S. X., Mai, Y.-W., and Cotterell, B., 1990, "Plastic η-factor (η_p) of Fracture Specimens with Deep and Shallow Cracks," *International Journal of Fracture*, Vol. 45, pp. 1~18.